Thermal Mineralization of Perfluorooctanesulfonic Acid (PFOS) to HF, CO_2 and SO_2

Nathan H. Weber[a], Cameron S. Delva[a], Sebastian P. Stockenhuber[b], Charles C. Grimison[c], John A. Lucas[c], John C. Mackie[a], Michael Stockenhuber[a] and Eric M. Kennedy[a]*.*

[a] Discipline of Chemical Engineering, School of Engineering, University of Newcastle, Callaghan, NSW, 2308, AUSTRALIA.

[b] Department of Chemistry, University College London, London, UK

[c] Ventia Services Pty Ltd, North Sydney NSW 2060, AUSTRALIA

Abstract

Utilizing air (O_2) as the bath gas at reaction temperatures between 500 – 1000 °C, the thermal decomposition of perfluorooctanesulfonic acid (PFOS) in an α-alumina reactor was studied. It was found that in an air bath gas (and in the absence of water vapor), COF_2 and trace amounts of C_2F_4 were detected. Quantum chemical calculations at the G4MP2 level of theory confirmed that CF_2 radicals can react with O_2 to form COF_2 and an O (^3P) atom.

The inclusion of 2000 ppmv or 20000 ppmv of water vapor ($H_2O_{(g)}$) to the air bath gas proved to be the key step to mineralizing all PFOS into HF, CO_2 and SO_2. At temperatures above 850 °C (0.95 – 0.84 s residence time), a feed of 20000 ppmv of $H_2O_{(g)}$ in air was observed to produce a product stream in which no gaseous fluorocarbon products were detected, with only HF, SO_2 and CO_2 being produced. A sulfur balance confirmed that 100±5% of all the S in PFOS had converted into SO_2 with a chemical kinetic model predicting in excess of 99.99999% destruction removal efficiency of PFOS at temperatures above 700 °C. Furthermore, from an elementary balance of F and C atoms, it was determined that at 1000 °C, approximately 99±5%

of F atoms present in PFOS have been converted into HF, and approximately 100±5% of C atoms had converted into CO_2.

A chemical kinetic model was developed to understand the importance of both O_2 and water vapor in the overall thermal decomposition of PFOS, leading to complete mineralization. In the presence of both O_2 and $H_2O_{(g)}$, it was found that relatively high concentrations of OH radicals were produced, with significant contribution to OH formation attributed to the well-known chain branching reaction $O(^3P) + H_2O \rightarrow OH + OH$.

Introduction

Per- and Poly-Fluoroalkyl Substances (PFAS) represent some of the most notorious contaminants found in the environment. PFAS stability, a result of the stable C-F bonds in their structure and the significant level of their usage, have caused numerous contamination sites worldwide.[1-3] One of the more problematic compounds in the PFAS group of products is perfluorooctanesulfonic acid (PFOS), a C8 fluorocarbon with a sulfonic acid head group. PFOS has been detected in soils, water, wildlife and even humans, and PFOS is associated with health and environmental concerns, which have prompted many jurisdictions to introduce legislation related to the legacy of these sites.[4-13] As a consequence, this has led to significant interest in developing technologies to remediate PFAS from the environment.

Thermal decomposition is one of the leading treatment methods, and this process generally comprises operation of two distinct and critical elevated temperature stages.[14] The first stage adopted to thermally remediate PFAS from a solid (e.g., soil), typically uses a rotary dryer operating between 200 and 700 °C, leading to the desorption of PFAS into the gas phase. The now exiting concentrated PFAS gas stream enters the second stage, which is generally a high temperature reactor (above 900 °C) used to thermally decompose the PFAS into HF, CO_2 and SO_2. The second stage has been studied by the USEPA, using the so-called combustor

"Rainbow furnace", where both CHF_3 and C_2F_6 had a destruction efficiency of over 99%.[15] Most thermal treatment methods aim to mineralize all the PFAS into HF, CO_2 and SO_2 and avoid undesirable fluorocarbons products. Additionally, with thermal treatment plants (thermal desorption plants) being built or currently operating, it is critical that the thermal decomposition of PFOS is well understood.[16]

Under inert conditions, PFOS was initially found to decompose into hydrogen fluoride (HF), sulfur dioxide (SO_2) and perfluorooctanyl fluoride ($C_8F_{16}O$).[17-19] However, our most recent inert gas pyrolysis study[20] found that tetrafluoroethylene (C_2F_4) was also produced from the thermal decomposition of PFOS. This led to the discovery of a previously undetected fission route for PFOS into C_8F_{17} and $HOSO_2$ radicals. The C_8F_{17} radical was found to fission into CF_2 radicals and directly into C_2F_4. Additionally, $C_8F_{16}O$ was also found to fission into FCO and C_7F_{15}, which will also rapidly fission into CF_2 radicals, which rapidly form C_2F_4 in inert conditions. For the $HOSO_2$ radical, it was found to decompose and form OH and SO_2.[20]

With the knowledge that CF_2 radicals will be produced in significant concentration, and noting that PFOS contains only one hydrogen (H) atom, a further study[21] was carried out under pyrolysis conditions with water vapor ($H_2O_{(g)}$) (in a helium bath gas). The objective of this study was to ascertain whether water vapor could provide the requisite H and O atoms needed to form both HF and CO_2 as the principal products. It was found that in the presence of excess $H_2O_{(g)}$, there was a significant increase in the concentration of HF, CO, and CO_2. Under the conditions studied, COF_2 was not detected. A quantum chemical study disclosed direct reactions between CF_2 and H_2O and CF_2 and OH, which are the major reactions steps during PFOS thermal decomposition in the presence of water vapor. However, co-pyrolysis of PFOS and water vapor alone was not able to convert all of the PFOS into HF and CO_2.[21]

Since air or oxygen are commonly present in most thermal treatment technologies, it is vital to understand the impact that O_2 has on the thermal decomposition of PFOS. Likewise, both O_2 and $H_2O_{(g)}$ are commonly present in commercial reactors; hence, insights are needed to understand the reactions influencing a feed containing air and $H_2O_{(g)}$.

The present investigation examined the effect that a feed gas containing air and combined air and $H_2O_{(g)}$ will have on the thermal decomposition of PFOS at different temperatures and residence times. To elucidate the influence that air and $H_2O_{(g)}$ have on the thermal decomposition of PFOS, we have studied a select number of reactions using quantum chemical techniques and as a result, extended our existing chemical kinetic model[20, 21] with the incorporation of new reactions involving O_2. This study provides much needed insight into the effect that air and combined air and $H_2O_{(g)}$ have on the thermal decomposition of PFOS.

Experimental

The experimental methodology is based on our previous study with the thermal decomposition of PFOS in the presence of water vapor.[21] However, instead of using helium as a bath gas, an air feed (78.1% N_2, 20.9% O_2 and 0.9% Ar) was used. Air was used separately as well as being bubbled through a saturator filled with Milli-Q water at 20 °C to make a combined air and water vapor bath gas. The combined bath gas was then diluted using a second controlled flow of air to produce a bath gas with a concentration of $H_2O_{(g)}$ between 1000 – 20000 ppmv. The experimental details have been discussed in depth in previous publications.[19-22] However, the experimental schematic and additional information related to the experimental methodology used has been added to the SI.

Computational methodology

Gaussian 09[23] has been used to study the interaction between O_2 and the important CF_2 and CF_3 radicals produced in the thermal decomposition of PFOS. Further reaction with O_2, OH

and H_2O of the radicals subsequently formed has also been studied. Molecular geometries of reactants, products and transition states (TSs) were obtained at the B3LYP/6-31G(2df,p) level of theory and energies were calculated by the high level G4MP2 method. Intrinsic reaction coordinate (IRC) analysis was used to link the TSs to their reactant(s) and product(s).

All relevant rate constants were calculated through the ChemRate program[24], which uses thermochemical parameters evaluated quantum chemically. Hindered rotors were identified and treated as such in the rate constant calculations, and canonical variation transition (CVT) state methods[25] were used for barrierless reactions. The Ansys Chemkin 2022 R1[26] model from our $H_2O_{(g)}$ and PFOS[27] was used to model the plug flow reactor (PFR) based on the experimental methodology with the relevant O_2 equations added.

Results and discussion

The thermal decomposition of PFOS using air as the carrier gas at atmospheric pressure was significantly different to the product distribution observed in our previous pyrolysis[19, 20] and $H_2O_{(g)}$ studies[27]. In the presence of air or under conditions where there is excess oxygen, the main products at temperatures above 600 °C were COF_2, SO_2, CO_2 and HF. A reduction in C_2F_4 concentration was evident from the FT-IR spectra in Figure 1.

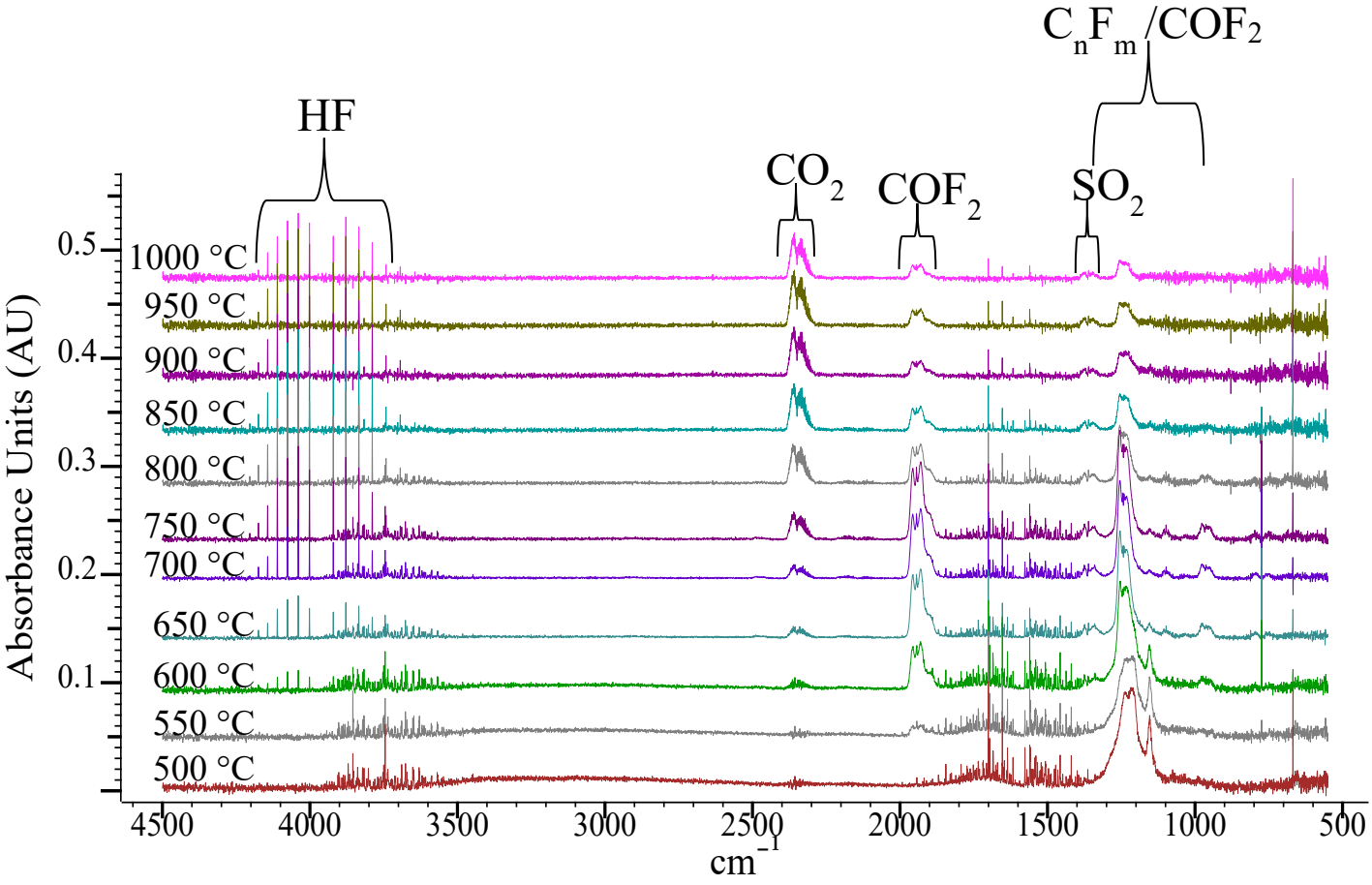

Figure 1. FT-IR spectra of PFOS thermal decomposition in an air bath gas between 500 – 1000 °C at a 150 mL min^{-1} (1.5 – 0.85 s) in a α-alumina reactor.

At 700 °C, COF_2 was the primary reaction product detected. We suggest that the slight decrease in COF_2 concentration at 750 °C is caused by a small amount of $H_2O_{(g)}$ (200 – 400 ppmv) present as an impurity in the gas supply. Our previous work[27] disclosed that even a low concentration of $H_2O_{(g)}$ can reduce the concentration of COF_2 produced at elevated temperatures. CO_2 and CO were also observed at high concentrations above 750 °C, which is

further evidence that $H_2O_{(g)}$ is reducing the concentration of COF_2 detected at elevated temperatures. However, even though there is a reduced concentration of gaseous fluorocarbon products, C_2F_4 and C_2F_6 are still detected. GC/MS was able to confirm the presence of longer chain perfluoroalkanes and perfluoroalkenes in the product stream. For the complete GC/MS table, please refer to the SI. The presence of fluorocarbon in the product gas stream is not surprising as an insufficient concentration of H atoms is present to form HF as the only fluorinated product. Nevertheless, using air as the reactor atmosphere does indicate that a combination of air and $H_2O_{(g)}$ might be the key to the full mineralization of PFOS into HF, CO_2 and SO_2. We now attempt to identify the reactions which assist in the mineralization in the presence of both O2 and H2O using quantum chemical analysis and kinetic modeling.

CF_2 reaction with O_2

Reaction between air/oxygen and PFOS at elevated temperatures in the absence of water vapor results in the production of COF_2 and inhibits the formation of C_2F_4. The addition of even trace quantities of water vapor reduces the concentration of COF_2 in the product stream and continues to inhibit the formation of C_2F_4. The addition of excess quantities of $H_2O_{(g)}$ leads to the absence of COF_2 in the product stream.

Molecular oxygen does not readily react with stable molecules. This is largely because of the strength of the O=O bond. The exception to this is the reaction $RH + O_2 \rightarrow HO_2 + R$. Reaction enthalpies for O_2 abstractions from C-H and COO-H to form HO_2 are typically 200 kJ mol^{-1} with A-factors around 10^{13} cm^3 mol^{-1} s^{-1} making the bimolecular initiation to HO_2 uncompetitive with the previously identified pyrolysis initiation reactions.[28, 29] However, this reaction has a large activation energy and a relatively low *A*-factor since most R-H bonds are strong. Thus, even in the presence of O_2, it is probable that the initiation of pyrolysis takes place in the same way as under an inert bath gas.

It is postulated that an initiation reaction takes place, as for inert gas pyrolysis, producing significant quantities of CF_2. The following reaction, where $O(^3P)$ denotes an oxygen atom in its ground (triplet state) and O_2 ($^3\Sigma_g$) denotes a ground state molecule of oxygen if it occurs as written

$$CF_2 + O_2\ (^3\Sigma_g) \rightarrow COF_2 + O\ (^3P) \qquad \text{(R1)}$$

is remarkable in that it has a large exothermicity of 163.9 kJ mol^{-1} (enthalpy values from Active Thermochemical tables[30]), and thermochemistry predicts that it is able to cleave the O=O bond to produce the highly reactive O (^3P) atom in a facile manner. Reaction (R1) would account for the inhibition of C_2F_4 formation and an increase in the concentration of COF_2. This is not an extensively studied reaction, with little definitive information available in the NIST Database[28]. Therefore, we have carried out a quantum chemical analysis of this reaction using the G4MP2 method.

Firstly, we located a TS for the reaction between $CF_2 + O_2$ ($^3\Sigma_g$) on the triplet surface. This has a barrier (at 298 K) of only 77.9 kJ mol^{-1}. However, an intrinsic reaction coordinate (IRC) analysis indicated that the TS does not directly link to the products, COF_2 + O (^3P), but to the triplet complex, CF_2OO. A potential energy scan of the O-O bond in the complex revealed an extremely weak O-O bond. In fact, the barrier to rupture to COF_2 + O (^3P) was only 8.1 kJ mol^{-1}. The reaction PES is shown in Figure 2.

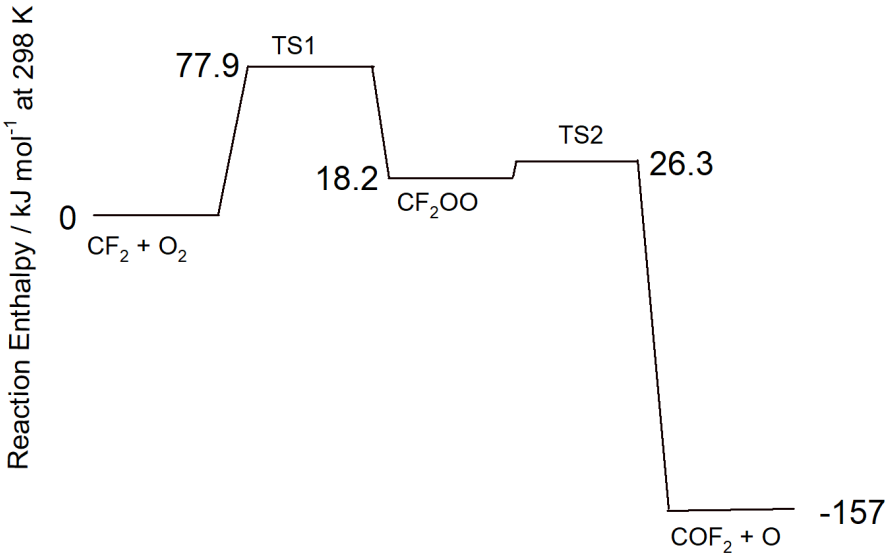

Figure 2. PES on the triplet surface for the reaction between CF_2 and O_2.

The interpretation of Figure 2 is as follows: Once the reactants, CF_2 and O_2, have sufficient energy to overcome the barrier represented by TS1, on account of the large exothermicity and minute barrier for decomposition, except at extremely low temperatures, the reaction will proceed all the way to products COF_2 + O and we can treat the reaction as the simple bimolecular reaction given by R1. Hence, we derive the forward rate constant for R1 as k_{1f} = $3.68 \times 10^5\ T^{2.050}$ exp(-73.22 kJ mol^{-1}/RT) cm^3 mol^{-1} s^{-1} and for the reverse rate constant, k_{1r} = $4.08 \times 10^9\ T^{1.316}$ exp(-240.0 kJ mol^{-1}/RT) cm^3 mol^{-1} s^{-1}. Tunneling plays an important role in determining the magnitude of the A-factor. The tunneling correction factor ranges from 5.2 at 500 K to 1.7 at 1500 K.

With R1 producing O (^{3}P) and in the presence of H_2O, the well-known chain branching reaction R2 can take place

$$O + H_2O \rightarrow OH + OH \qquad (R2)$$

which forms OH radicals critical to the thermal decomposition of PFOS. It should be noted that the reaction between O atoms and CF_2 radicals to form COF_2 is spin-forbidden hence will not regenerate this product.

CF_3 reaction with O_2

CF_3 radicals play a minor role in the decomposition of PFOS as the product of their recombination, C_2F_6, is usually detected in low concentration (below 50 ppmv) in the product stream. In the presence of water vapor or oxygen, CF_3 radicals can undergo several reactions.

The reaction between CF_3 and $^3O_2$ (R3) has been studied because of its importance in the upper atmosphere. The NIST Chemical Kinetic Database[28] lists many measurements of the rate constant for

$$CF_3 + O_2\ (+M) \rightarrow CF_3OO\ (+M) \qquad (R3)$$

M is a third-body collision partner, usually the carrier gas. When shown in a reaction as (+M) this denotes a reaction in "fall-off", i.e., the reaction rate is dependent on the pressure of the collider. Most data have been obtained around 300 K and lower temperatures. At 1 atm and 300 K, the reaction is bimolecular. In their 1997 review, Atkinson et al.[31] recommended an experimental value of $k_3 = 6.03 \times 10^{12}$ cm^3 mol^{-1} s^{-1} for the reaction at temperatures between 200 – 400 K. The only high temperature value is a theoretical one obtained by Cobos and Troe[32] of $k_3 = 1.56 \times 10^{13} \exp(-2.59\ \text{kJ mol}^{-1}/RT)$ cm^3 mol^{-1} s^{-1}. At 400 K this gives a rate constant of 7.15×10^{12} cm^3 mol^{-1} s^{-1} so agreement between theory and experiment would appear to be good.

CF_3OO radicals

To the best of our knowledge, there are no kinetic data on the possible reaction of CF_3OO radicals with water. Hence, we have carried out a quantum chemical study at the G4MP2 level of theory for the reaction

$$CF_3OO + H_2O \rightarrow CF_3OOH + OH \qquad (R4)$$

This reaction occurs on the doublet surface. A TS was located for R4, and a barrier of 115.6 kJ mol^{-1} at 298 K was obtained. However, the reaction enthalpy at 298 K was found to be 118.0 kJ mol^{-1} at this same level of theory. An intrinsic reaction coordinate (IRC) analysis revealed that the product was the post-reaction complex (PRC) $CF_3OOH\_OH\_prc$ located at 87.2 kJ mol^{-1} above the reactants. This is illustrated in the PES shown in Figure 3.

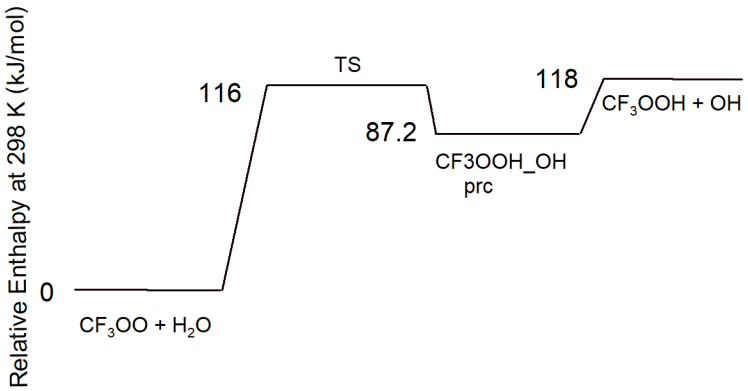

Figure 3. PES for reaction between CF_3OO and H_2O.

Hence, the effective barrier for the formation of CF_3OOH + OH is equal to the reaction enthalpy of 118.0 kJ mol^{-1}. The rate constant for R4 is evaluated with this barrier and the thermodynamic constants of the located TS. A value of $k_4 = 5.62\ T^{3.528}$ exp(-113.3 kJ mol^{-1}/RT) $cm^3\ mol^{-1}\ s^{-1}$ was obtained by ChemRate.

The hydrocarbon analogue of CF_3OOH, viz., CH_3OOH, has been much studied and is known to undergo barrierless fission to CH_3O + OH, with an activation energy similar to the bond

enthalpy and an *A*-factor between 6×10^{14} and 4×10^{15} s^{-1}.[33] Hence a reasonable value of the rate constant for R5

$$CF_3OOH \rightarrow CF_3O + OH \qquad (R5)$$

would be $k_5 = 2 \times 10^{15} \exp(-205 \text{ kJ mol}^{-1}/RT)$ s^{-1} where the activation energy is taken to be equal to the enthalpy of reaction at 298 K.

In the presence of water and air (and probably even in water alone), there are likely to be significant quantities of OH radicals, so the reaction between CF_3OO and OH radicals could be important. Only a single value has been obtained (Biggs et al.[34]) for the rate constant purported to be for the reaction

$$CF_3OO + OH \rightarrow CF_3O + HO_2 \qquad (R6)$$

However, products were not detected but inferred, and the reactant CF_3OO underwent parallel unimolecular decomposition, making rate measurements of the bimolecular R6 difficult to unravel. Biggs et al.[34] obtained the sole value of 2.4×10^{13} cm^3 mol^{-1} s^{-1} at 296 K. More recently, Du and Zhang[35] carried out a quantum chemical study of the CF_3OO + OH reaction system, showing that the mechanism was far more complex than given by R6 but did not provide any rate data. They point out that a reaction between these two radicals can occur both on singlet and triplet surfaces.

We carried out a similar quantum chemical study but at a higher level (G4MP2) than that undertaken by Du and Zhang[35], whose calculations were made at the b3lyp/6-311G(d,p) level of theory. There are several similarities with their earlier results, but also some important differences. The reaction between the two radicals leads to a CF_3OOOH product on both singlet and triplet surfaces, but the structures and stabilities of CF_3OOOH-sing and CF_3OOOH-trip differ considerably. These structures are depicted in Figure 4.

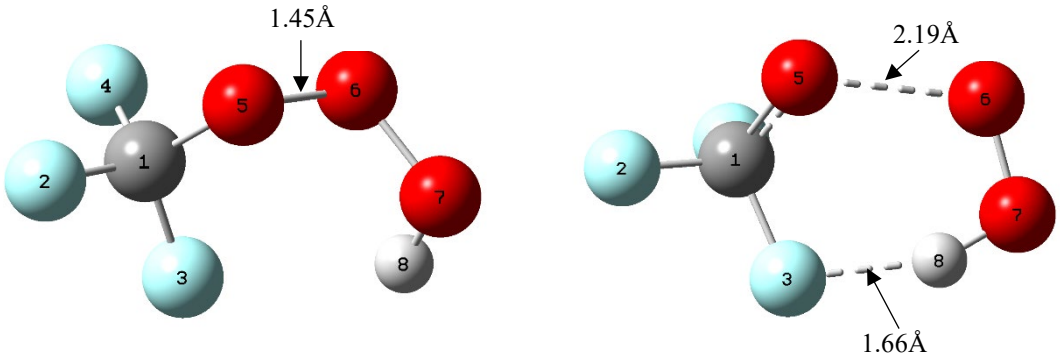

Figure 4. Optimized structures of CF_3OOOH. Singlet (left), Triplet (right).

The CF_3OOOH-sing is very stable, lying 137.9 kJ mol^{-1} below the reactants, whereas the triplet product lay just 22.05 kJ mol^{-1} below the reactants at 298 K. (In comparison, Du and Zhang[35] obtained values of -130.71 and -82.59 kJ mol^{-1}, respectively.) The optimized geometries were not substantially different from those of Du and Zhang[35]. However, Du and Zhang[35] described both CF_3OOOH products as biradicals, whereas the singlet in the present study appeared to be a closed shell and its counterpart, a pure triplet. Contamination with higher spin states appeared to be low, with the largest observed value of $\langle S^2 \rangle = 2.0083$ prior to annihilation of spin contaminant in the triplet case and $\langle S^2 \rangle = 0.7529$ for doublets. Hence, the application of the single reference methods used in the present study would seem to be appropriate.

Triplet CF_3OOOH forms a weakly bonded six-membered ring which could almost be described as a post-reaction complex between CF_3O and HO_2 radicals. Separated $CF_3O + HO_2$ lie at -17.5 kJ mol^{-1} with respect to the reactants CF_3OO and OH. Du and Zhang[35] do not report the observation of a TS on either surface for the reaction between CF_3OO and OH. However, we

located a TS for the reaction between these two radicals on the triplet surface. At 298 K, this TS has a barrier of 84.8 kJ mol^{-1}, but it does *not* link with $CF_3O + HO_2$ on the products' side. Instead, an IRC shows that the product is CF_3OOOH-trip.

We located a TS for the fission of the triplet into $CF_3O + HO_2$, which lies just 1.38 kJ mol^{-1} above the triplet. However, the reaction enthalpy is calculated as 4.6 kJ mol^{-1}, slightly larger than the calculated barrier. This might indicate that the products could be a very weakly bound post-reaction complex, but the probable accuracy of the G4MP2 method is between ± 4.2 – 6.3 kJ mol^{-1}. Hence, it is probably best to describe this "barrier" as virtually barrierless.

Again, a TS beginning with the triplet CF_3OOOH has been located, for the elimination of HF + COF_2, i.e.,

$$CF_3OOOH \rightarrow COF_2 + HF + {}^3O_2 \qquad \text{(R7)}$$

The G4MP2 evaluation of this barrier encountered convergence problems in the coupled cluster singles and doubles (CCSD) route of the compound calculation, so only an estimate of -2.5 ± 5.0 kJ mol^{-1} could be obtained. It should be noted that Du and Zhang[35] also obtained a small negative value for this barrier. They also obtained a TS of approximately 167 kJ mol^{-1} directly from $CF_3OO + OH$ for the formation of $CF_3OH + {}^3O_2$. Because of its height, this process plays no part in the overall reaction mechanism, nor do the large barrier processes they located for the singlet reaction surface.

The PES on the triplet surface is depicted in Figure 5.

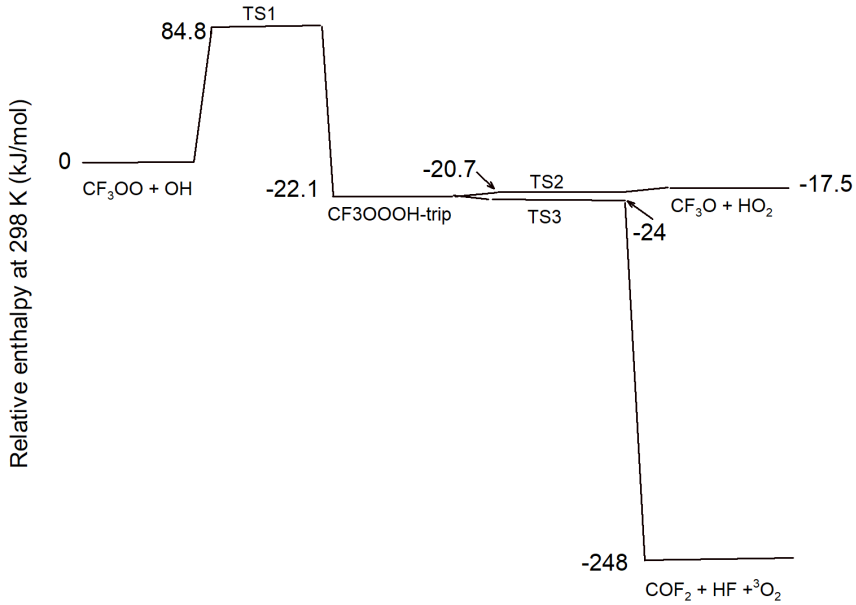

Figure 5. PES for reaction between CF_3OO and OH. TS1 is for formation of the triplet CF_3OOOH. TS2 is for formation of $CF_3O + HO_2$ from the triplet and TS3 is for elimination of HF and $^3O_2$.

Examination of the PES in Figure 5 leads to the conclusion that the two routes, viz., to $CF_3O + HO_2$ and to $COF_2 + HF + {}^3O_2$ will be facile and have the same rate constants, determined by the thermodynamic parameters of the reactants and TS1. Hence, the rate constants of k_6 and k_8 where

$$CF_3OO + OH \rightarrow [CF_3OOOH\text{-trip}] \rightarrow COF_2 + HF + {}^3O_2 \qquad (R8)$$

are $k_6 = k_8 = 1.05\times10^3\ T^{2.587} \exp(-81.88\ \text{kJ mol}^{-1}/RT)\ \text{cm}^3\ \text{mol}^{-1}\ \text{s}^{-1}$.

With the now better understanding of the impact that O_2 will have on the thermal decomposition of PFOS, we have updated our kinetic model to include reactions involving O_2. All new reactions added to the kinetic model are provided in Table 1.

Table 1. New reactions added to the kinetic model (see SI)

Equation	A-factor*	n	E_a/R (K)	Reference
$CF_2 + O_2 = COF_2 + O$	6.68×10^5	2.05	7800	PW
$CF_3 + O_2 + M = CF_3O_2 + M$	1.56×10^{13}	0	314	PW
$O + CO (+M) <=> CO_2 (+M)$	1.80×10^{10}	0.329	1200	[36]
$O_2 + CO <=> O + CO_2$	2.50×10^{12}	0	24053	[36]
$2H + CO_2 <=> H_2 + CO_2$	5.50×10^{20}	-2	0	[36]
$2O + M <=> O_2 + M$	1.20×10^{17}	-1	0	[36]
$O + H + M <=> OH + M$	5.00×10^{17}	-1	0	[36]
$O + H_2 <=> H + OH$	3.87×10^4	2.70	3150	[36]
$H + O_2 <=> O + OH$	5.06×10^{15}	-0.49	8102	[37]
$2OH <=> O + H_2O$	8.5×10^4	2.26	-898	[36]

*Rate constant, $k = A\ T^n \exp(-E_a/RT)$. Units vary for depending on the order of the reaction. s^{-1} for first order, cm^3/mol s for second order and cm^6/mol^2 s for third order reactions. PW – Present Work.

Air and water experiments

Based on our previous work, water vapor alone, especially excess water vapor, significantly reduced the rate of COF_2 formation.[27] Experiments indicate that COF_2 is the main product in an air atmosphere. Consequently, if we combined both air and $H_2O_{(g)}$ in the feed, it is plausible that at elevated temperatures, only HF, CO_2 and SO_2 will be observable products.

Figures 6 and 7 depict FT-IR spectra of products obtained with combined air and $H_2O_{(g)}$ between 500 – 1000 °C, with Figure 6 having a reduced $H_2O_{(g)}$ concentration of 2000 ppmv while Figure 7 has 20000 ppmv of $H_2O_{(g)}$.

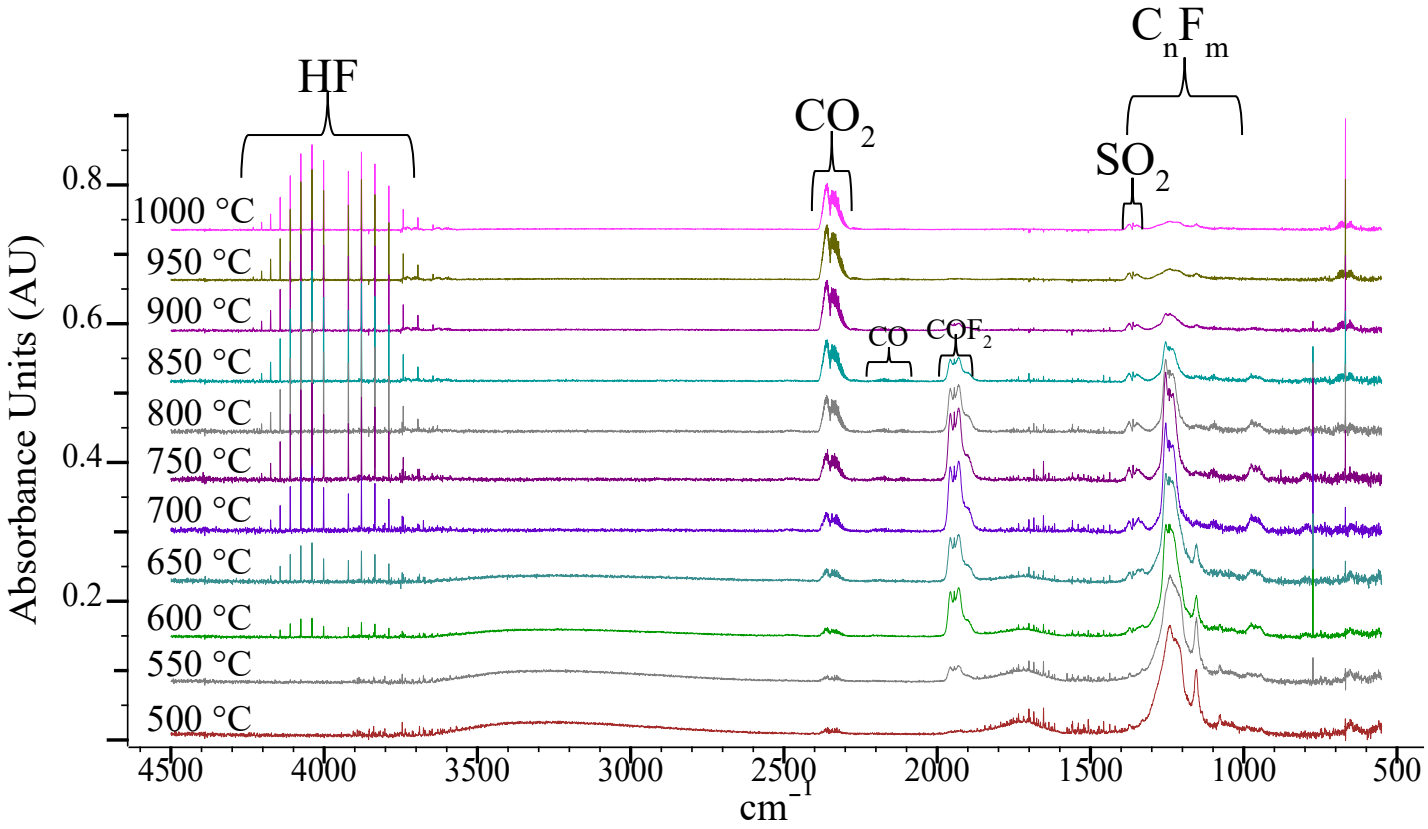

Figure 6. FT-IR spectra of PFOS thermal decomposition in the presence of 2000 ppmv of $H_2O_{(g)}$ between 500 – 1000 °C using a 150 mL min^{-1} air bath gas giving a residence time of 1.5 – 0.85 s.

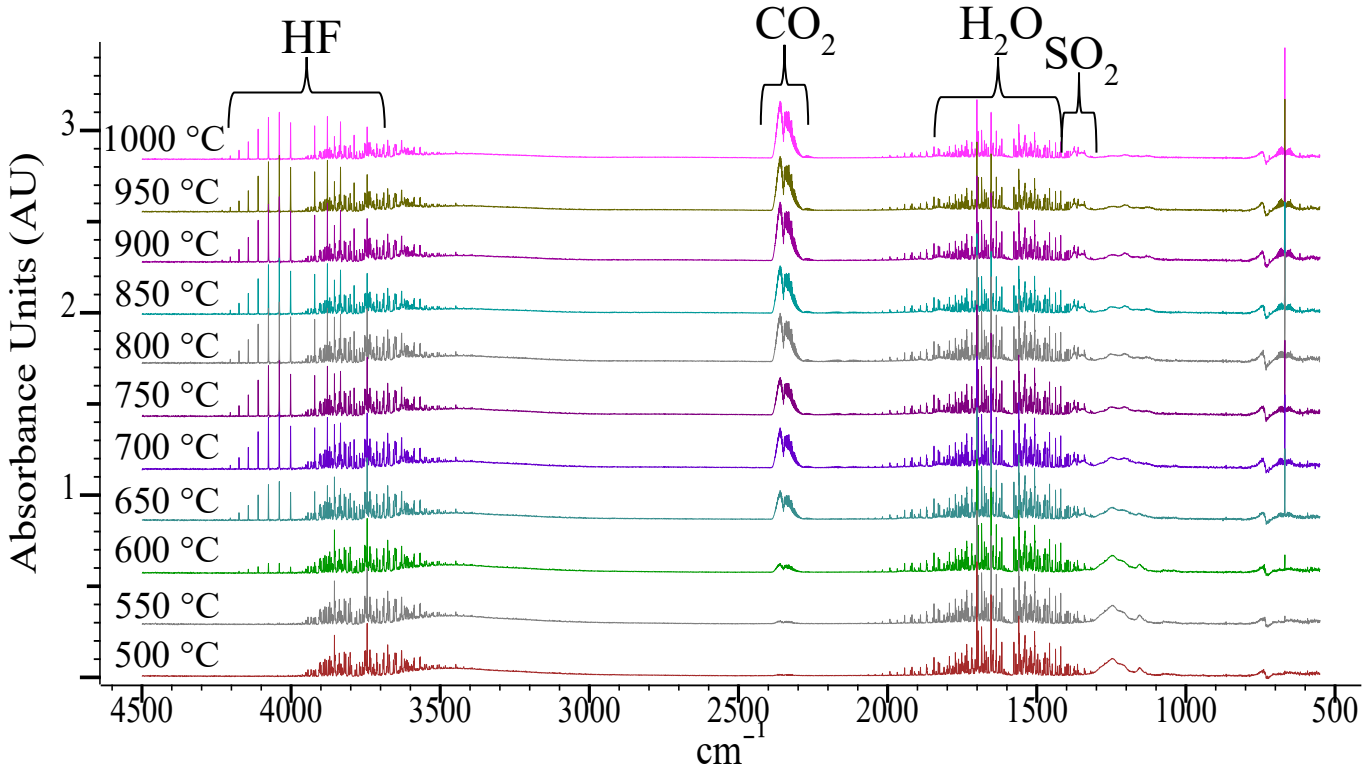

Figure 7. FT-IR spectra of PFOS thermal decomposition in the presence of 20000 ppmv of $H_2O_{(g)}$ between 500 – 1000 °C using a 150 mL min^{-1} air bath gas giving a residence time of 1.5 – 0.85 s.

The reduced (2000 ppmv) $H_2O_{(g)}$ and air runs (Figure 6) have similar FT-IR spectra to the spectra of air (Figure 1) between 500 – 800 °C. This is anticipated as both have limited amounts of $H_2O_{(g)}$ present; however, as the temperature exceeds 800 °C, it is clear that the extra $H_2O_{(g)}$ can convert more fluorocarbons to HF and CO_2. Moreover, in excess $H_2O_{(g)}$ and air (Figure 7), there was a minimal concentration of fluorocarbons between 500 – 1000 °C, with HF and CO_2 being the primary products detected over the entire temperature range studied. It was also found that at temperatures above 850 °C, fluorocarbons were not detected, indicating that all the PFOS had decomposed into HF, CO_2 and SO_2.

To assist in understanding the process that is involved in the thermal decomposition of PFOS in the presence of air and $H_2O_{(g)}$, the concentration of HF, CO_2 and SO_2 were modeled under various reaction conditions using Chemkin 2022 R1. These concentrations are plotted as mole ratios (concentration ratios) versus temperature at a flowrate of 150 mL min^{-1} and depicted in Figure 8.

a)

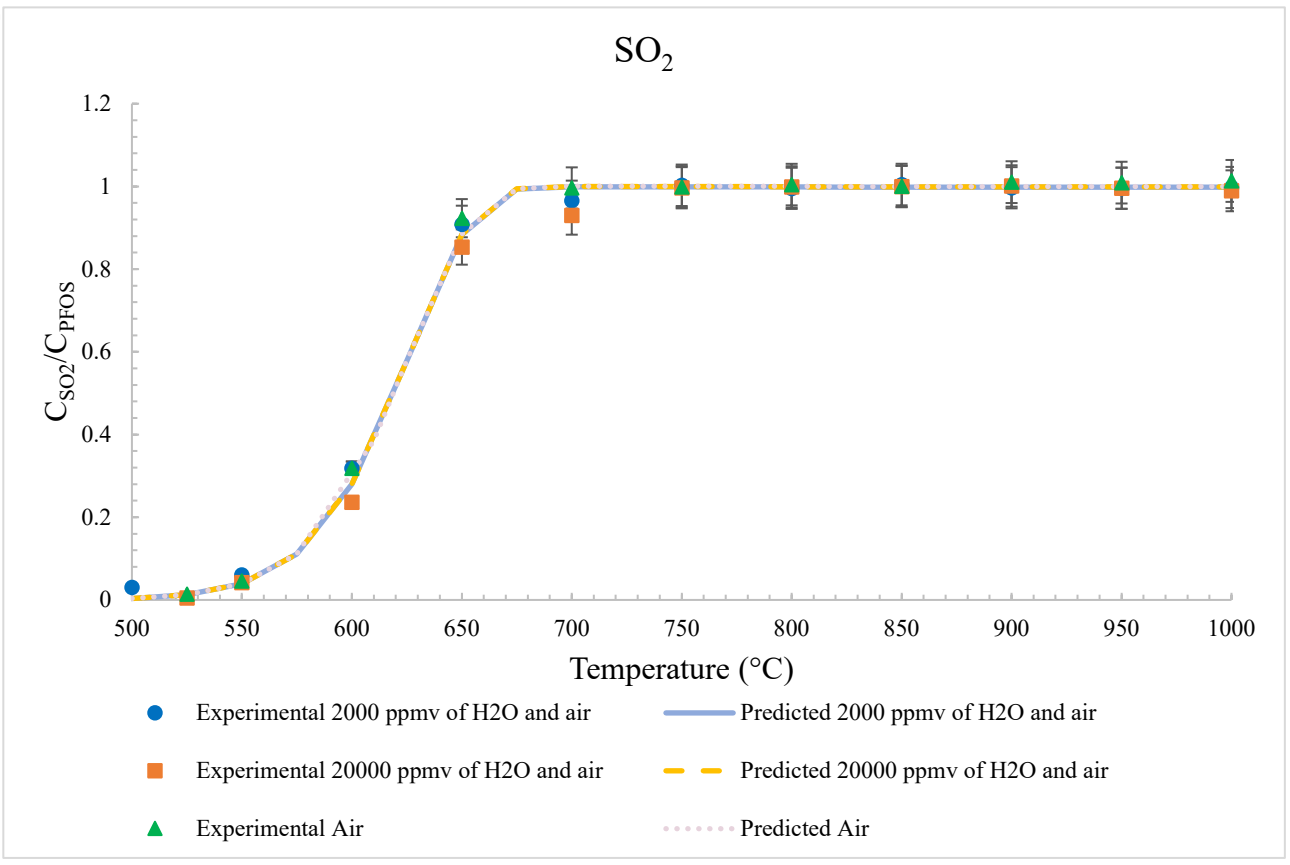

b)

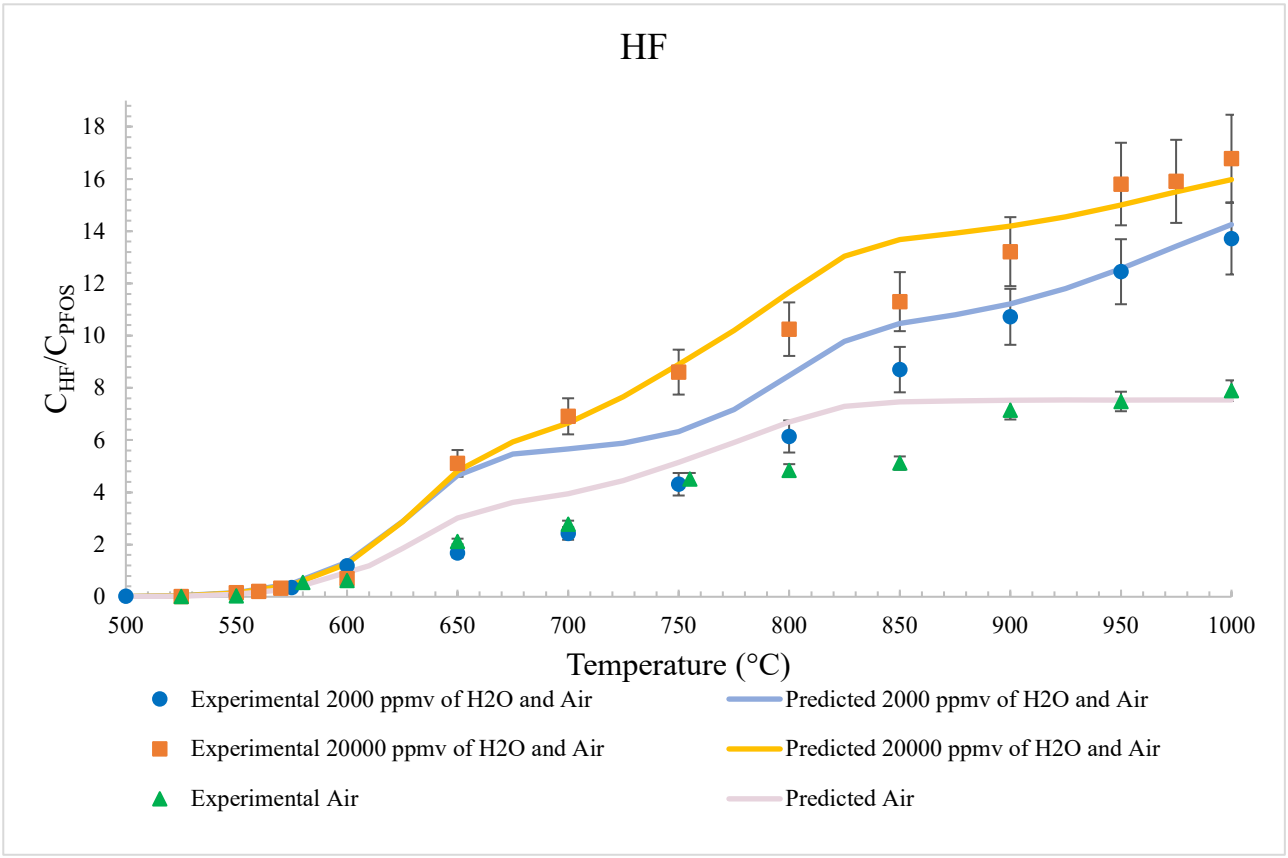

c)

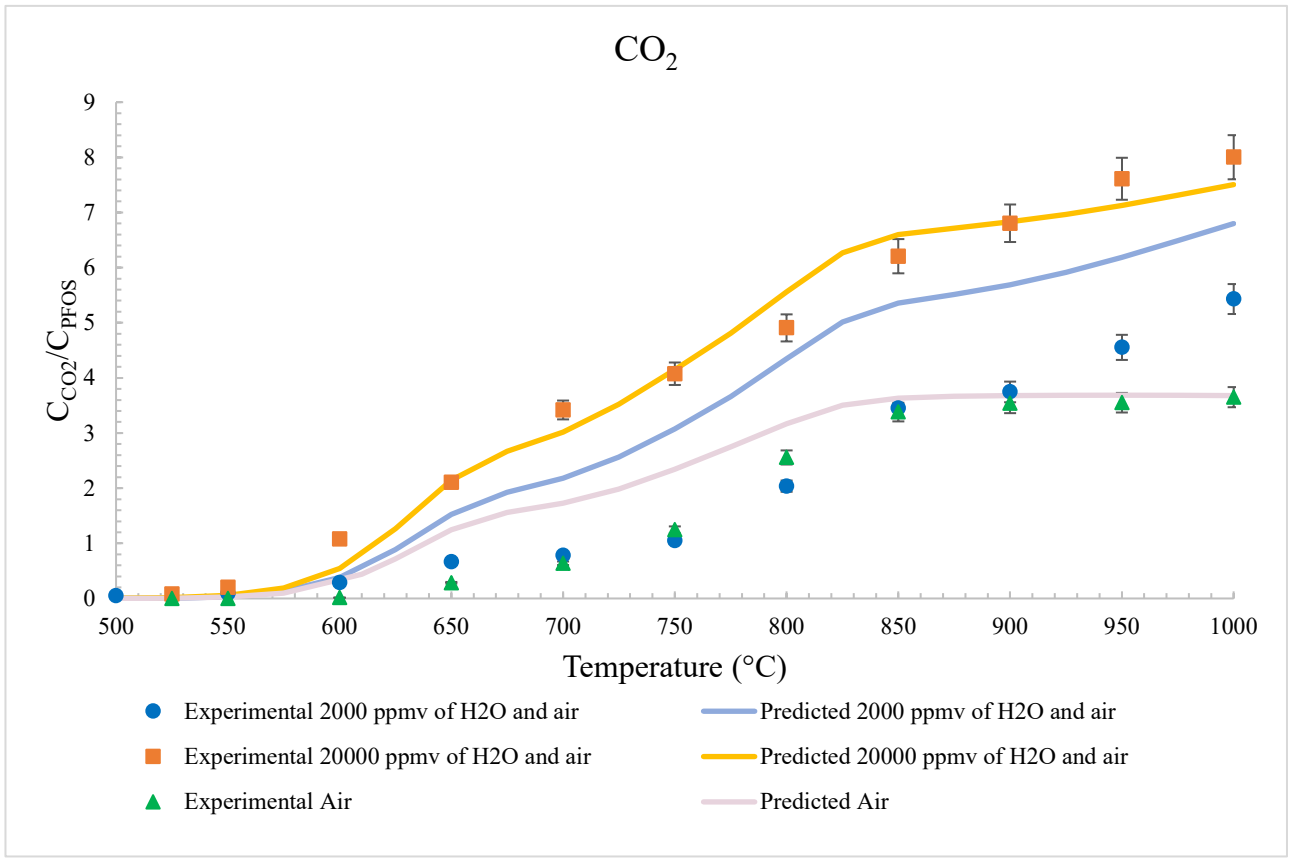

Figure 8. The predicted (line) and the experimental (points) of the thermal decomposition of PFOS using air as the bath gas at 150 mL min^{-1} (1.5 – 0.85 s) for experimental (green triangles, 169 ppmv of PFOS) and predicted (light green, 169 ppmv of PFOS) and in the presence of 2000 ppmv of $H_2O_{(g)}$ for predicted (light blue, 169 ppmv of PFOS) and experimental (blue circle, 178 ppm of PFOS), alongside the 20000 ppmv of $H_2O_{(g)}$ for predicted (light orange, 178 ppmv of PFOS), and experimental (orange square, 179 ppm of PFOS. a) Mole ratio (concentration ratio) of the total SO_2 concentration and total PFOS concentration. b) Mole ratio (concentration ratio) of the total HF concentration and total PFOS concentration. c) Mole ratio (concentration ratio) of the total CO_2 concentration and total PFOS concentration.

The predicted SO_2 concentration from the model (Figure 8a) is in excellent agreement with experimental data.

The experimentally measured HF/PFOS concentration ratio (Figure 8b) reached 16.8 F atoms converted into HF out of a total of 17 in the PFOS feed (99±5% conversion) in the presence of air and 20000 ppmv of $H_2O_{(g)}$ at 1000 °C. It is probable that the conversion is higher; however, the precision of the experimental technique is limited to ±5%.

There are three distinct temperature ranges that impact the overall thermal decomposition of PFOS in excess $H_2O_{(g)}$ and air. Between 500 – 600 °C, the thermal decomposition of PFOS into HF and SO_2 at equimolar rates is observed, which has been described in our inert gas pyrolysis experiments.[19, 20] Between 600 – 850 °C, CF_2 radicals are the primary product and these species will react predominantly with OH radicals and, to some extent O_2 which leads to the formation of additional HF. At temperatures above 850 °C, the overall mechanism produces excess concentration of OH radicals, which readily react with CF_2, with only a small amount of O_2 reacting directly with CF_2 radicals. This leads to the formation of HF and CO_2 as the primary products. Although the model predicts that some COF_2 will be present at 1000 °C, it is not observed experimentally. COF_2 can react directly with $H_2O_{(g)}$[38, 39]; however, the model still predicts COF_2 to be present. Uchimaru et al.[40] suggested that excess $H_2O_{(g)}$ will likely reduce the barrier needed to decompose COF_2 owing to the participation of an extra H_2O in the reaction TS which could explain the limits in the model.

The combined air mixed with a reduced level of $H_2O_{(g)}$ (2000 ppmv) compared to the "dry" air experiments produced similar trends up to 800 °C. This is most likely due to the presence of $H_2O_{(g)}$, which forms more OH radicals at the elevated temperatures needed to react with CF_2, thus producing HF. Overall, a similar trend is observed between 2000 and 20000 ppmv of $H_2O_{(g)}$, resulting in approximately 80% of all F present in PFOS converted into HF at 1000

°C. Between 600 – 800 °C, more than double the number of F atoms are converted into HF under conditions where there is a significant excess of $H_2O_{(g)}$ in the feed. During experiments at the lower level of 2000 ppmv of $H_2O_{(g)}$ feed, there is competition between O_2 and OH to react with CF_2 whereas, with excess water vapor, reaction with CF_2 is dominated by its reaction with OH alone, highlighting the importance of excess $H_2O_{(g)}$ in the feed. It was also observed at temperatures below 850 °C, in both 2000 and 20000 ppmv of $H_2O_{(g)}$, that fluorocarbons, especially C_2F_4, C_2F_6 and COF_2 are still detected. This was even more evident at lower water vapor concentrations (2000 ppmv) This implies, between 600 – 850 °C, it should be expected that short chain fluorocarbons will be produced, and careful consideration needs to be made what temperature to choose when thermally decomposing PFOS.

The CO_2 concentration profile (Figure 8c) has a very similar trend to HF formation in the combined air and 20000 ppmv of $H_2O_{(g)}$ runs. It was discovered that of the eight C atoms present in PFOS, all eight were converted to CO_2 (100±5%) in full agreement with model predictions up to and above 900 °C. Furthermore, it was also found that the HF to CO_2 ratio was between 2 and 2.15 at temperatures above 650 °C in both the model and experiment, which is reflective of the ratio of F atoms to C atoms in PFOS of 2.125.

Reaction path diagrams between PFOS and HF and PFOS and CO_2 are provided in SI. A similar trend was also observed for the flowrate of 122 mL min^{-1}, which can be found in the SI.

Importance of OH radicals, H and O atoms

As described in our previous publication, where we examined the effect of water vapor on PFOS decomposition[27], there were only limited chain branching reactions to form OH. This led to reactions such as R9,[36] ensuring that the OH concentration was relatively low.

$$CO + OH \rightarrow CO_2 + H \qquad (R9)$$

However, with O_2 in the feed, additional chain branching reactions, most notably R1, R2 and R10, result in a significant enhancement in the concentration of OH from O atoms.

$$H + O_2 \leftrightarrow O + OH \quad \text{(R10)}$$

To understand the full extent of the impact that the combined water vapor and air have on the thermal decomposition of PFOS, the rate of production of O and H atoms alongside OH radicals in the middle of the reactor, as calculated by chemkin is provided in Figure 9. Please refer to the SI for points from the start and end of the reactor.

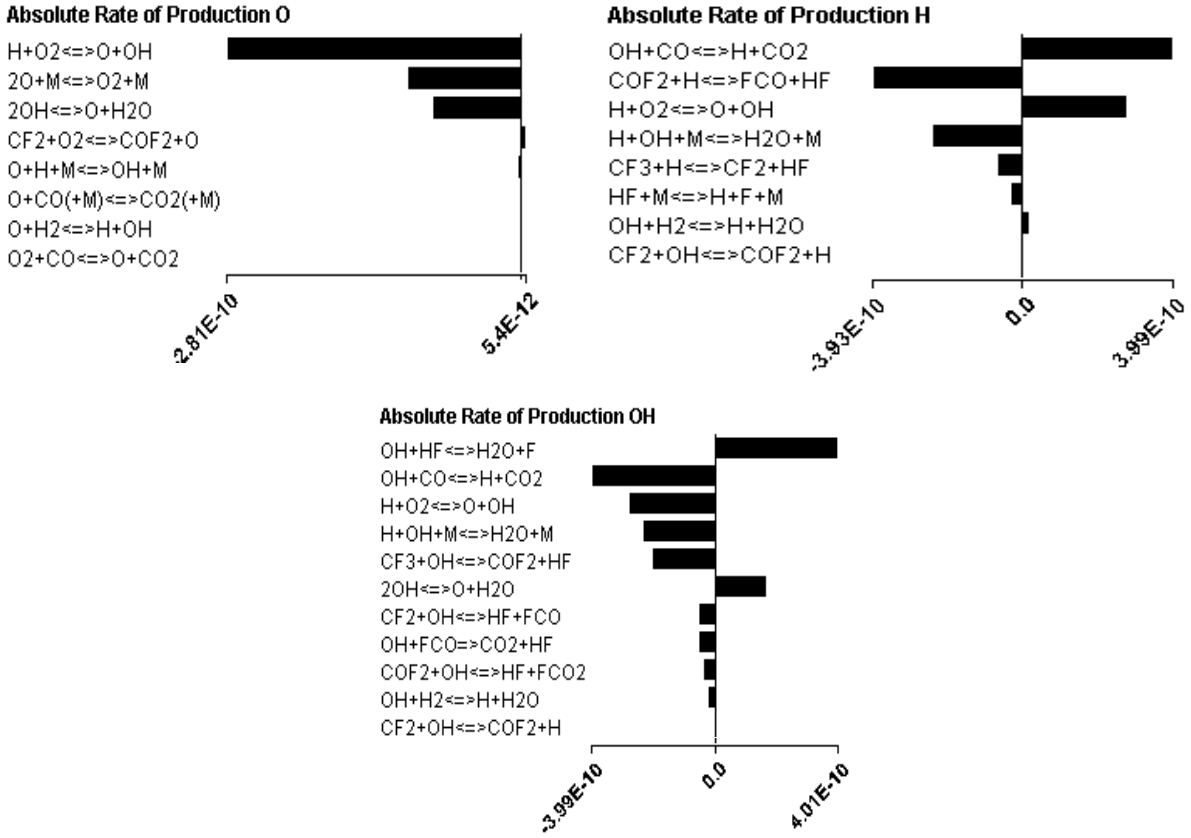

Figure 9. The absolute ratio of production of O, H and OH at 900 °C within 9 cm of reaction (0.47 s residence time) provided by Ansys Chemkin

As expected, the primary reactions leading to the production of O atoms are via both R1 and R10 in the first 0 - 2 cm (0 – 0.11 s residence) of the reactor, which leads to the chain formation of OH via R2. R2 between 0 – 3.24 cm of the reactor (0 to 0.16 s residence time at 900 °C) was the dominant producer of OH.

Upon closer inspection, the FCO radical is the principal propagator of OH, where it is well known that FCO radical breakdown takes place via R11.

$$FCO + M \rightarrow F + CO + M \quad (R11)$$

while the F atoms via the reverse of R12

$$OH + HF \leftrightarrow H_2O + F \quad (R12)$$

will form HF and more OH radicals. For the remaining residence time and length of the reactor, the combination of R11 and R12 is the primary way that OH radicals are produced.

As mentioned in our previous publication[27], most FCO radicals will form via R14

$$CF_2 + OH \leftrightarrow HF + FCO \quad (R14)$$

However, with the addition of O_2 enhancing the concentration of OH, R9 will also readily produce more H atoms. These H atoms are vital to decomposing all the COF_2 into more FCO through R15.

$$COF_2 + H \leftrightarrow HF + FCO \quad (R15)$$

R15 forms more FCO, which produces more OH and H atoms. It is also important to note that some of the H and OH will be terminated by forming H_2O.

Without both O_2 and $H_2O_{(g)}$ present in the thermal decomposition of PFOS, there would be a very limited amount of OH formed, which would lead to the formation of fluorocarbons. A full sensitivity analysis for OH is provided in the SI.

Summary of the effect of reaction conditions on the PFOS decomposition products formed

Understanding the effect that reaction conditions have on PFOS decomposition provides critical information relevant to the industrial development of thermal treatment processes of

PFAS. During reaction at temperatures between 500 and 600 °C, the initial stage of thermal decomposition of PFOS occurs. The primary products are essentially the same during reaction under various conditions resulting in the formation of HF and SO_2. At temperatures above 600 °C, differences are observed in product distribution between each reactor bath gas composition. This difference is associated with CF_2 radical formation and subsequent reaction. Table 2 provides a summary of all the major products in the temperature range of 500 °C – 1000 °C and reactor conditions of inert pyrolysis, $H_2O_{(g)}$, air and a combined air and $H_2O_{(g)}$ feed.

It is expected that in most industrial processes designed to treat PFAS, such as PFOS, the bath gas will include both air and $H_2O_{(g)}$. Table 2 provides a summary of the products that have been detected during reactions in such conditions. Consequently, understanding the mechanism of the thermal decomposition of PFOS can provide the knowledge needed for the thermal treatment of PFAS in order to optimize the process and have a better awareness of safety requirements.

Table 2. A summary of the expected main products in the thermal decomposition of PFOS at different reactor conditions and temperature ranges.

Temperature range (°C)	**Pyrolysis[19, 20] (Helium bath gas)**	**Excess Water vapor ($H_2O_{(g)}$) and Helium**	**Air**	**Air + excess $H_2O_{(g)}$**
500 – 600 (Initial thermal decomposition of PFOS)	HF, SO_2, $C_8F_{16}O$ and C_2F_4	HF, SO_2, $C_8F_{16}O$ and C_2F_4	HF, SO_2, $C_8F_{16}O$ and COF_2	HF, SO_2, and CO_2
600 – 700 (Increase CF_2 radical concentration)	HF, SO_2, $C_8F_{16}O$ and C_2F_4	HF, SO_2, $C_8F_{16}O$, C_2F_4 and COF_2	HF, SO_2, $C_8F_{16}O$ and COF_2	HF, SO_2, COF_2 and CO_2
700 – 850 (All PFOS has decomposed)	HF, SO_2, $C_8F_{16}O$, C_2F_4 and CO	HF, SO_2, $C_8F_{16}O$, C_2F_4, CO and CO_2	HF, SO_2, $C_8F_{16}O$ and COF_2	HF, SO_2, and CO_2
850 – 1000 (C_2F_4 breakdowns and OH radicals become dominate in $H_2O_{(g)}$)	HF, SO_2, C_2F_4, CO, CO_2 and perfluoroalkanes and perfluoroalkenes	HF, SO_2, CO, CO_2, perfluoroalkanes and perfluoroalkenes	HF, SO_2, COF_2, CO and CO_2	HF, SO_2, and CO_2

Destruction and Removal Efficiency (DRE)

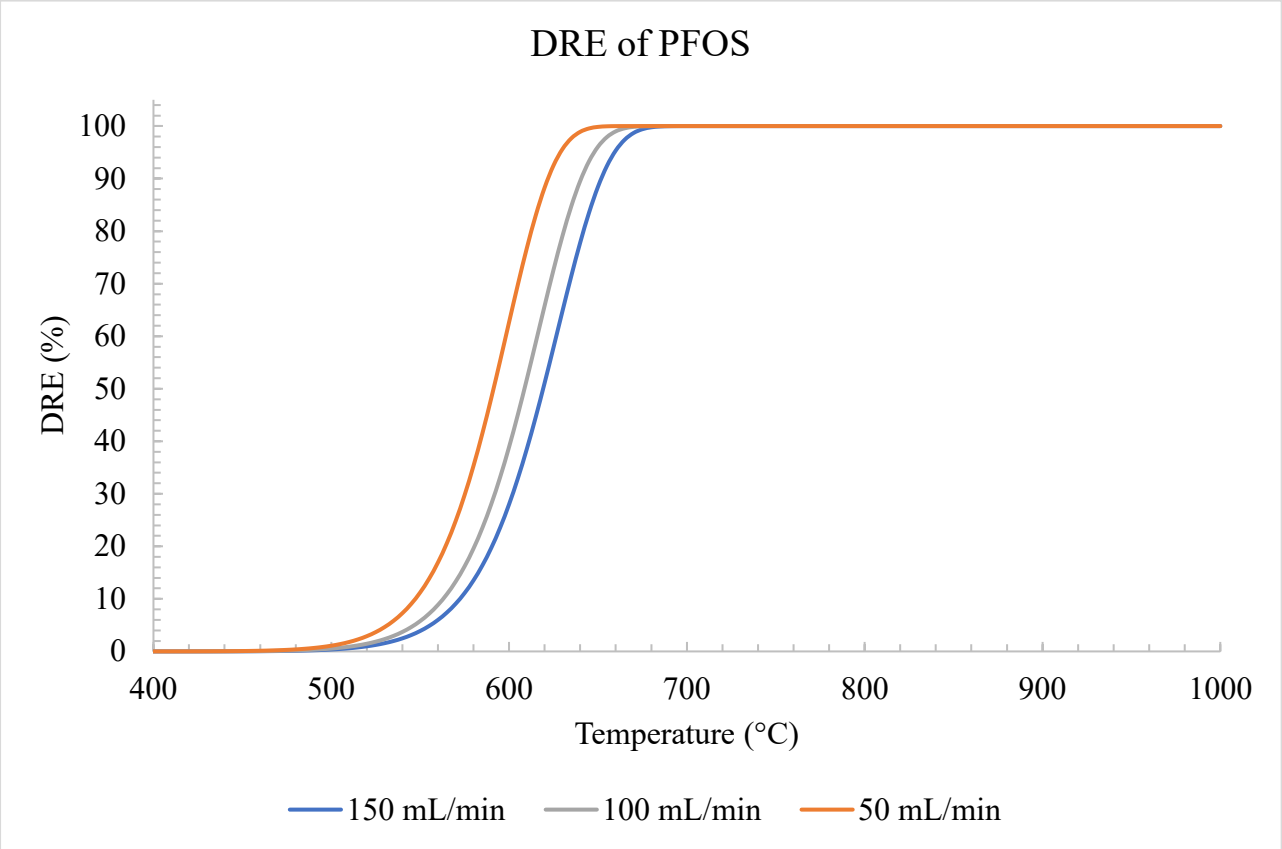

Figure 10. DRE of PFOS modeled in Chemkin based on the experimental parameters of 200 ppmv of PFOS, blue line 150 mL min^{-1} (1.5 – 0.85 s), grey line 100 mL min^{-1} (2.4 – 1.3 s) and orange line 50 mL min^{-1} (4.8 – 2.5 s) in inert helium, air, water vapor and combined air and water vapor.

Impact of the $H_2O_{(g)}$ and O_2 ratio

The impact of $H_2O_{(g)}/O_2$ has been examined by our kinetic model at various $H_2O_{(g)}$ and O_2 concentrations. It was evident that excess $H_2O_{(g)}$ is needed; however, the modeling did indicate that a restricted concentration of O_2 can provide more HF than in excess O_2 (higher ratio of H_2O to O_2). Figure 11 illustrates a surface 3D plot of the modeled different concentrations of O_2 and $H_2O_{(g)}$ and the impact it has on the conversion of HF.

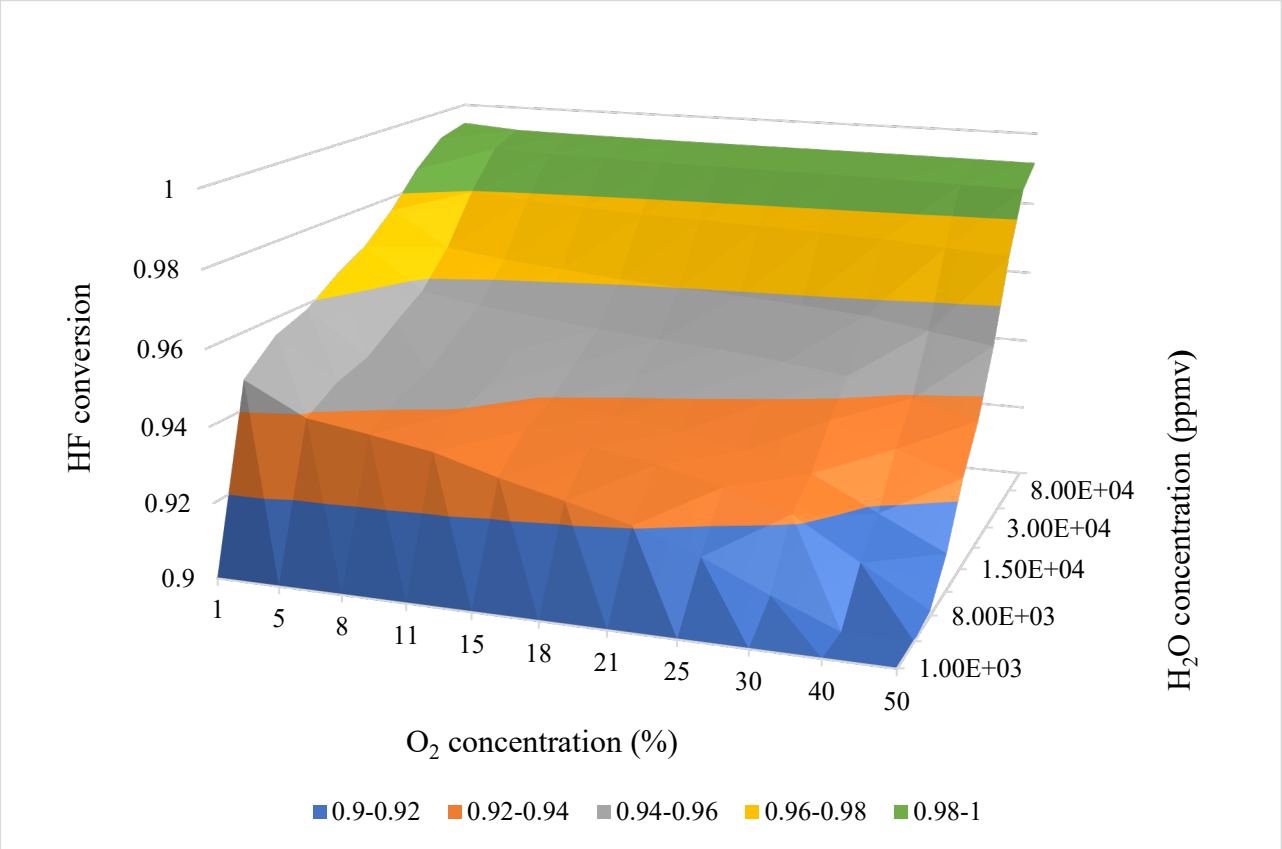

Figure 11. 3D surface plot based on the modeling of the different concentrations of O_2 and $H_2O_{(g)}$ in Chemkin at 50 mL min^{-1} at 1000 °C (2.54 s residence time) . The O_2 concentration is plotted as the total percentage present in bath gas. Times by 10000 to get ppmv.

150 mL min^{-1} and 100 mL min^{-1} flowrates are provided in the SI. Having a longer residence time and less O_2 provided more conversion into HF, whereas with a shorter residence time, higher O_2 concentration is needed for higher HF conversion.

As mentioned previously, this is not fully reflective of the experimental conditions as there is still limited understanding of the mechanism of the reaction between COF_2 and $H_2O_{(g)}$, especially on alumina surfaces. Nevertheless, ratios similar to those modeled will lead to significant mineralization, i.e., formation of HF, CO_2 and SO_2.

Conclusion

The thermal decomposition of PFOS using air (O_2) as a carrier gas was found to produce COF_2 as the primary product; consequently, the C_2F_4 concentration as a reaction product significantly decreased. Quantum chemical calculations at the G4MP2 level of theory found that the CF_2 radicals produced within the thermal decomposition of PFOS readily react with O_2 to form COF_2 and an O atom.

Using a combination of air and excess water vapor as the bath gas in the experimental trials, the thermal decomposition of PFOS produced three main products of HF, SO_2 and CO_2. Furthermore, at temperatures above 850 °C, it was found that only these three products were observable, and at 1000 °C (0.85 s residence time), ≈99% conversion of F mineralized PFOS into HF and 100% of C into CO_2. Using a reduced water vapor concentration of 2000 ppmv and air produced an 80% conversion to HF, revealing the importance of excess water vapor. A chemical kinetic model (82 elementary reaction steps and 43 species) predicted a similar trend to the experimental results and demonstrated the importance air and $H_2O_{(g)}$ have on the product distribution in the thermal decomposition of PFOS. The presence of both air and $H_2O_{(g)}$ in the feed leads to the formation of significant amounts of OH radicals, the key reactant needed to form HF and CO_2 from the thermal decomposition of PFOS. The formation of OH radicals was found to arise from two primary sources. The first is a direct reaction between $H_2O_{(g)}$ and F atoms forming OH and HF. The second is from the presence of $O(^3P)$ atoms which produce two OH radicals from a chain branching reaction with $H_2O_{(g)}$. $O(^3P)$ atoms are, in turn,

generated by the reaction of O_2 with CF_2 and a separate reaction between O_2 and H atoms forming more OH and an O atom. Without air and excess $H_2O_{(g)}$, limited OH radicals are produced, allowing for other fluorocarbons products to be created.

Overall, combined air (O_2) and excess water vapor and temperatures above 850 °C as reaction conditions provide an inexpensive source of H, OH and O that can mineralize all PFOS into HF, CO_2 and SO_2. Hence, this study provides crucial insights into the entire thermal decomposition of PFOS and the role CF_2 radicals play in the presence of water vapor and air.

ASSOCIATED CONTENT

Supporting information.

Expanded experimental and schematic

GC/MS methodology and table

Predicted (model) and experimental thermal decomposition of PFOS in the presence of air and water vapor concentration graphs for 122 mL min^{-1}

Reaction path diagrams between PFOS and HF and CO_2

Rate of production and sensitive analysis

H_2O/O_2 ratio 3D surface graphs

Kinetic model for thermal decomposition of PFOS table

NASA thermochemical coefficients for Chemkin modelling

PFOS concentration calculation example

Acknowledgements

This research was funded by the Australian Research Council

This work was supported through Ventia Services Pty Ltd and Veolia and Ventia Joint Venture.

Ventia Services Pty Ltd and EarthSure (a Veolia Ventia Joint Venture)

AUTHOR INFORMATION

Corresponding author

*Corresponding author Eric Kennedy

Phone: (+61 2) 4985 4422

Email: eric.kennedy@newcastle.edu.au

Mailing address: College of Engineering, Science and Environment, Discipline of Chemical Engineering, School of Engineering, University of Newcastle, Callaghan NSW 2308, Australia

*John Mackie

Phone: (+61 2) 4985 4439

Email: john.mackie@newcastle.edu.au

Mailing address: College of Engineering, Science and Environment, Discipline of Chemical Engineering, School of Engineering, University of Newcastle, Callaghan NSW 2308, Australia

Author contributions

The manuscript was written through contributions of all authors. All authors have given approval to the final version of the manuscript.

Conflict of interest

There are no conflicts to declare.

References

(1) Montero-Campillo, M. M.; Mora-Diez, N.; Lamsabhi, A. M., Thermodynamic Stability of Neutral and Anionic PFOS: A Gas-Phase, n-Octanol, and Water Theoretical Study. *The Journal of Physical Chemistry A* **2010,** *114* (37), 10148-10155.

(2) Li, Y.; Fletcher, T.; Mucs, D.; Scott, K.; Lindh, C. H.; Tallving, P.; Jakobsson, K., Half-lives of PFOS, PFHxS and PFOA after end of exposure to contaminated drinking water. *Occup Environ Med* **2018,** *75* (1), 46-51.

(3) Key, B. D.; Howell, R. D.; Criddle, C. S., Fluorinated Organics in the Biosphere. *Environmental Science & Technology* **1997,** *31* (9), 2445-2454.

(4) Sunderland, E. M.; Hu, X. C.; Dassuncao, C.; Tokranov, A. K.; Wagner, C. C.; Allen, J. G., A review of the pathways of human exposure to poly- and perfluoroalkyl substances (PFASs) and present understanding of health effects. *J. Expo. Sci. Environ. Epidemiol.* **2019,** *29* (2), 131-147.

(5) Ding, N.; Harlow, S. D.; Randolph Jr, J. F.; Loch-Caruso, R.; Park, S. K., Perfluoroalkyl and polyfluoroalkyl substances (PFAS) and their effects on the ovary. *Human Reproduction Update* **2020,** *26* (5), 724-752.

(6) Shearer, J. J.; Callahan, C. L.; Calafat, A. M.; Huang, W.-Y.; Jones, R. R.; Sabbisetti, V. S.; Freedman, N. D.; Sampson, J. N.; Silverman, D. T.; Purdue, M. P.; Hofmann, J. N., Serum Concentrations of Per- and Polyfluoroalkyl Substances and Risk of Renal Cell Carcinoma. *JNCI: Journal of the National Cancer Institute* **2020,** *113* (5), 580-587.

(7) Banwell, C.; Housen, T.; Smurthwaite, K.; Trevenar, S.; Walker, L.; Todd, K.; Rosas, M.; Kirk, M., Health and social concerns about living in three communities affected by per- and polyfluoroalkyl substances (PFAS): A qualitative study in Australia. *PLOS ONE* **2021,** *16* (1), e0245141.

(8) Cordner, A.; De La Rosa, V. Y.; Schaider, L. A.; Rudel, R. A.; Richter, L.; Brown, P., Guideline levels for PFOA and PFOS in drinking water: the role of scientific uncertainty, risk assessment decisions, and social factors. *J Expo Sci Environ Epidemiol* **2019,** *29* (2), 157-171.

(9) Castiglioni, S.; Valsecchi, S.; Polesello, S.; Rusconi, M.; Melis, M.; Palmiotto, M.; Manenti, A.; Davoli, E.; Zuccato, E., Sources and fate of perfluorinated compounds in the aqueous environment and in drinking water of a highly urbanized and industrialized area in Italy. *Journal of Hazardous Materials* **2015,** *282*, 51-60.

(10) Tian, Y.; Zhou, Y.; Miao, M.; Wang, Z.; Yuan, W.; Liu, X.; Wang, X.; Wang, Z.; Wen, S.; Liang, H., Determinants of plasma concentrations of perfluoroalkyl and polyfluoroalkyl substances in pregnant women from a birth cohort in Shanghai, China. *Environment International* **2018,** *119*, 165-173.

(11) Giesy, J. P.; Kannan, K., Global Distribution of Perfluorooctane Sulfonate in Wildlife. *Environmental Science & Technology* **2001,** *35* (7), 1339-1342.

(12) European Chemicals Agency Perfluoroalkyl chemicals (PFAS). https://echa.europa.eu/hot-topics/perfluoroalkyl-chemicals-pfas (accessed 10/06/2022). 2022.

(13) PFAS Action Act of 2021. https://www.congress.gov/bill/117th-congress/house-bill/2467 (accessed 12/06/2022). 2021.
(14) Wang, J.; Lin, Z.; He, X.; Song, M.; Westerhoff, P.; Doudrick, K.; Hanigan, D., Critical Review of Thermal Decomposition of Per- and Polyfluoroalkyl Substances: Mechanisms and Implications for Thermal Treatment Processes. *Environmental Science & Technology* **2022,** *56* (9), 5355-5370.
(15) Krug, J. D.; Lemieux, P. M.; Lee, C.-W.; Ryan, J. V.; Kariher, P. H.; Shields, E. P.; Wickersham, L. C.; Denison, M. K.; Davis, K. A.; Swensen, D. A.; Burnette, R. P.; Wendt, J. O. L.; Linak, W. P., Combustion of C1 and C2 PFAS: Kinetic modeling and experiments. *Journal of the Air & Waste Management Association* **2022,** *72* (3), 256-270.
(16) Veolia - Ventia Joint Venture EarthSure. https://www.ventia.com/page/earthsure-suez-and-ventia-joint-venture (accessed 18/06/2022). 2022.
(17) Khan, M. Y.; So, S.; da Silva, G., Decomposition kinetics of perfluorinated sulfonic acids. *Chemosphere* **2020,** *238*, 124615.
(18) Altarawneh, M., A chemical kinetic model for the decomposition of perfluorinated sulfonic acids. *Chemosphere* **2021,** *263*, 128256.
(19) Weber, N. H.; Stockenhuber, S. P.; Delva, C. S.; Abu Fara, A.; Grimison, C. C.; Lucas, J. A.; Mackie, J. C.; Stockenhuber, M.; Kennedy, E. M., Kinetics of Decomposition of PFOS Relevant to Thermal Desorption Remediation of Soils. *Industrial & Engineering Chemistry Research* **2021,** *60* (25), 9080-9087.
(20) Weber, N. H.; Delva, C. S.; Stockenhuber, S. P.; Grimison, C. C.; Lucas, J. A.; Mackie, J. C.; Stockenhuber, M.; Kennedy, E. M., Modeling and Experimental Study on the Thermal Decomposition of Perfluorooctanesulfonic Acid (PFOS) in an α-Alumina Reactor. *Industrial & Engineering Chemistry Research* **2022,** *61* (16), 5453-5463.
(21) Weber, N. H.; Delva, C. S.; Stockenhuber, S. P.; Grimison, C. C.; Lucas, J. A.; Mackie, J. C.; Stockenhuber, M.; Kennedy, E. M., Thermal Decomposition of Perfluorooctanesulfonic Acid (PFOS) in the Presence of Water Vapor. *Industrial & Engineering Chemistry Research* **2022**.
(22) Weber, N. H.; Stockenhuber, S. P.; Benhelal, E.; Grimison, C. C.; Lucas, J. A.; Mackie, J. C.; Stockenhuber, M.; Kennedy, E. M., Products and mechanism of thermal decomposition of chlorpyrifos under inert and oxidative conditions. *Environmental Science: Processes & Impacts* **2020,** *22* (10), 2084-2094.
(23) Frisch, M. J.; Trucks, G. W.; Schlegel, H. B.; Scuseria, G. E.; Robb, M. A.; Cheeseman, J. R.; Scalmani, G.; Barone, V.; Petersson, G. A.; Nakatsuji, H.; Li, X.; Caricato, M.; Marenich, A. V.; Bloino, J.; Janesko, B. G.; Gomperts, R.; Mennucci, B.; Hratchian, H. P.; Ortiz, J. V.; Izmaylov, A. F.; Sonnenberg, J. L.; Williams; Ding, F.; Lipparini, F.; Egidi, F.; Goings, J.; Peng, B.; Petrone, A.; Henderson, T.; Ranasinghe, D.; Zakrzewski, V. G.; Gao, J.; Rega, N.; Zheng, G.; Liang, W.; Hada, M.; Ehara, M.; Toyota, K.; Fukuda, R.; Hasegawa, J.; Ishida, M.; Nakajima, T.; Honda, Y.; Kitao, O.; Nakai, H.; Vreven, T.; Throssell, K.; Montgomery Jr., J. A.; Peralta, J. E.; Ogliaro, F.; Bearpark, M. J.; Heyd, J. J.; Brothers, E. N.; Kudin, K. N.; Staroverov, V. N.; Keith, T. A.; Kobayashi, R.; Normand, J.; Raghavachari, K.; Rendell, A. P.; Burant, J. C.; Iyengar, S. S.; Tomasi, J.; Cossi, M.; Millam, J. M.; Klene, M.; Adamo, C.; Cammi, R.; Ochterski, J. W.; Martin, R. L.; Morokuma, K.; Farkas, O.; Foresman, J. B.; Fox, D. J. *Gaussian 09 Rev. D.01*, Wallingford, CT, 2016.
(24) Mokrushin, V.; Bedanov, V.; Tsang, W.; Zachariah, M.; Knyazev, V.; McGivern, W. *ChemRate, version 1.5.10*, 2011.
(25) Garrett, B. C.; Truhlar, D. G., Generalized transition state theory. Classical mechanical theory and applications to collinear reactions of hydrogen molecules. *The Journal of Physical Chemistry* **1979,** *83* (8), 1052-1079.

(26) Ansys *Chemkin-Pro 2022 R1*, 2022 R1; 2022.
(27) Weber, N. H.; Delva, C. S.; Stockenhuber, S. P.; Grimison, C. C.; Lucas, J. A.; Mackie, J. C.; Stockenhuber, M.; Kennedy, E. M., Thermal Decomposition of Perfluorooctanesulfonic Acid (PFOS) in the presence of water vapor. 2022.
(28) J. A. Manion; R. E. Huie; R. D. Levin; D. R. Burgess Jr.; V. L. Orkin; W. Tsang; W. S. McGivern; J. W. Hudgens; V. D. Knyazev; D. B. Atkinson; E. Chai; A. M. Tereza; C.-Y. Lin; T. C. Allison; W. G. Mallard; F. Westley; J. T. Herron; R. F. Hampson; Frizzell, D. H., NIST Chemical Kinetics Database, NIST Standard Reference Database 17, Version 7.0 (Web Version),. National Institute of Standards and Technology: Gaithersburg, Maryland, 2015.
(29) Burcat, A.; Ruscic, B., *Third Millenium Ideal Gas and Condensed Phase Thermochemical Database for Combustion with Updates from Active Thermochemical Tables*. Argonne National Laboratory: 2005.
(30) Ruscic, B.; Bross, D. H. Active Thermochemical Tables (ATcT) values based on ver. 1.122r of the Thermochemical Network. ATcT.anl.gov. 2021.
(31) Atkinson, R.; Baulch, D. L.; Cox, R. A.; Hampson, R. F.; Kerr, J. A.; Rossi, M. J.; Troe, J., Evaluated Kinetic, Photochemical and Heterogeneous Data for Atmospheric Chemistry: Supplement V. IUPAC Subcommittee on Gas Kinetic Data Evaluation for Atmospheric Chemistry. *Journal of Physical and Chemical Reference Data* **1997,** *26* (3), 521-1011.
(32) Cobos, C. J.; Troe, J., Theory of thermal unimolecular reactions at high pressures. II. Analysis of experimental results. *The Journal of Chemical Physics* **1985,** *83* (3), 1010-1015.
(33) Baulch, D. L.; Cobos, C. J.; Cox, R. A.; Frank, P.; Hayman, G.; Just, T.; Kerr, J. A.; Murrells, T.; Pilling, M. J.; Troe, J.; Walker, R. W.; Warnatz, J., Evaluated Kinetic Data for Combustion Modeling. Supplement I. *Journal of Physical and Chemical Reference Data* **1994,** *23* (6), 847-848.
(34) Biggs, P.; E. Canosa-Mas, C.; E. Shallcross, D.; Vipond, A.; P. Wayne, R., Kinetics of the reactions of CF3O2 with OH, HO2 and H. *Journal of the Chemical Society, Faraday Transactions* **1997,** *93* (16), 2701-2705.
(35) Du, B.; Zhang, W., Ab initio quantum chemical studies on the reactions of CF3O2 with OH. *Chemical Physics* **2006,** *327* (1), 10-14.
(36) Gregory P. Smith; David M. Golden; Michael Frenklach; Nigel W. Moriarty; Boris Eiteneer; Mikhail Goldenberg; C. Thomas Bowman; Ronald K. Hanson; Soonho Song; William C. Gardiner, J.; Vitali V. Lissianski; Zhiwei Qin GRI-Mech 3.0. http://www.me.berkeley.edu/gri_mech/ (accessed 01/05/2022). 1999.
(37) Varga, T.; Olm, C.; Nagy, T.; Zsély, I. G.; Valkó, É.; Pálvölgyi, R.; Curran, H. J.; Turányi, T., Development of a Joint Hydrogen and Syngas Combustion Mechanism Based on an Optimization Approach. *International Journal of Chemical Kinetics* **2016,** *48* (8), 407-422.
(38) Farlow, M. W.; Man, E. H.; Tullock, C. W.; Richardson, R. D., Carbonyl Fluoride. In *Inorganic Syntheses*, 1960; pp 155-158.
(39) Zachariah, M. R.; Tsang, W.; Westmoreland, P. R.; Burgess, D. R. F., Theoretical Prediction of the Thermochemistry and Kinetics of Reactions of CF2O with Hydrogen Atom and Water. *The Journal of Physical Chemistry* **1995,** *99* (33), 12512-12519.
(40) Uchimaru, T.; Tsuzuki, S.; Sugie, M.; Tokuhashi, K.; Sekiya, A., Ab initio study of the hydrolysis of carbonyl difluoride (CF2O): importance of an additional water molecule. *Chemical Physics Letters* **2004,** *396* (1), 110-116.

TOC art